Monitoring photobleaching and hemodynamic responses to HPPH-mediated photodynamic therapy of head and neck cancer: a case report

Ulas Sunar,[1,*] Daniel Rohrbach,[1] Nestor Rigual,[2] Erin Tracy,[3] Ken Keymel,[1] Michele T. Cooper,[1] Heinz Baumann,[3] and Barbara H. Henderson[1]

[1]*Department of Cell Stress Biology, Roswell Park Cancer Institute, Buffalo, NY, 14263, USA*
[2]*Department of Head and Neck Surgery, Roswell Park Cancer Institute, Buffalo, NY, 14263, USA*
[3]*Department of Molecular and Cellular Biology, Roswell Park Cancer Institute, Buffalo, NY, 14263, USA*
**ulas.sunar@roswellpark.org*

Abstract: We present initial results obtained during the course of a Phase I clinical trial of 2-1[hexyloxyethyl]-2-devinylpyropheophorbide-a (HPPH)-mediated photo-dynamic therapy (PDT) in a head and neck cancer patient. We quantified blood flow, oxygenation and HPPH drug photobleaching before and after therapeutic light treatment by utilizing fast, non-invasive diffuse optical methods. Our results showed that HPPH-PDT induced significant drug photobleaching, and reduction in blood flow and oxygenation suggesting significant vascular and cellular reaction. These changes were accompanied by cross-linking of the signal transducer and activator of transcription 3 (STAT3), a molecular measure for the oxidative photoreaction. These preliminary results suggest diffuse optical spectroscopies permit non-invasive monitoring of PDT in clinical settings of head and neck cancer patients.

©2010 Optical Society of America

OCIS codes: (170.0170) Medical optics and biotechnology; (170.3660) Light propagation in tissues; (170.6480) Spectroscopy, speckle; (170.3880) Medical and biological imaging.

References and links

1. www.cancer.gov/cancertopics/types/head-and-neck.
2. H. J. Feldmann, M. Molls, and P. Vaupel, "Blood flow and oxygenation status of human tumors," Strahlenther. Onkol. **175**(1), 1–9 (1999).
3. M. A. Biel, "Photodynamic therapy treatment of early oral and laryngeal cancers," Photochem. Photobiol. **83**(5), 1063–1068 (2007).
4. I. Georgakoudi, and T. H. Foster, "Singlet oxygen- versus nonsinglet oxygen-mediated mechanisms of sensitizer photobleaching and their effects on photodynamic dosimetry," Photochem. Photobiol. **67**(6), 612–625 (1998).
5. G. Yu, T. Durduran, C. Zhou, H. W. Wang, M. E. Putt, H. M. Saunders, C. M. Sehgal, E. Glatstein, A. G. Yodh, and T. M. Busch, "Noninvasive monitoring of murine tumor blood flow during and after photodynamic therapy provides early assessment of therapeutic efficacy," Clin. Cancer Res. **11**(9), 3543–3552 (2005).
6. D. A. Bellnier, W. R. Greco, G. M. Loewen, H. Nava, A. R. Oseroff, R. K. Pandey, T. Tsuchida, and T. J. Dougherty, "Population pharmacokinetics of the photodynamic therapy agent 2-[1-hexyloxyethyl]-2-devinyl pyropheophorbide-a in cancer patients," Cancer Res. **63**(8), 1806–1813 (2003).
7. B. W. Henderson, C. Daroqui, E. Tracy, L. A. Vaughan, G. M. Loewen, M. T. Cooper, and H. Baumann, "Cross-linking of signal transducer and activator of transcription 3--a molecular marker for the photodynamic reaction in cells and tumors," Clin. Cancer Res. **13**(11), 3156–3163 (2007).
8. W. Liu, A. R. Oseroff, and H. Baumann, "Photodynamic therapy causes cross-linking of signal transducer and activator of transcription proteins and attenuation of interleukin-6 cytokine responsiveness in epithelial cells," Cancer Res. **64**(18), 6579–6587 (2004).
9. U. Sunar, H. Quon, T. Durduran, J. Zhang, J. Du, C. Zhou, G. Yu, R. Choe, A. Kilger, R. Lustig, L. Loevner, S. Nioka, B. Chance, and A. G. Yodh, "Noninvasive diffuse optical measurement of blood flow and blood oxygenation for monitoring radiation therapy in patients with head and neck tumors: a pilot study," J. Biomed. Opt. **11**(6), 064021 (2006).
10. D. J. Pine, D. A. Weitz, P. M. Chaikin, and E. Herbolzheimer, "Diffusing wave spectroscopy," Phys. Rev. Lett. **60**(12), 1134–1137 (1988).
11. C. Cheung, J. P. Culver, K. Takahashi, J. H. Greenberg, and A. G. Yodh, "In vivo cerebrovascular measurement combining diffuse near-infrared absorption and correlation spectroscopies," Phys. Med. Biol. **46**(8), 2053–2065 (2001).

#126926 - $15.00 USD Received 13 Apr 2010; revised 21 Jun 2010; accepted 23 Jun 2010; published 29 Jun 2010
(C) 2010 OSA

12. J. P. Culver, T. Durduran, D. Furuya, C. Cheung, J. H. Greenberg, and A. G. Yodh, "Diffuse optical tomography of cerebral blood flow, oxygenation, and metabolism in rat during focal ischemia," J. Cereb. Blood Flow Metab. **23**(8), 911–924 (2003).
13. T. Durduran, R. Choe, G. Yu, C. Zhou, J. C. Tchou, B. J. Czerniecki, and A. G. Yodh, "Diffuse optical measurement of blood flow in breast tumors," Opt. Lett. **30**(21), 2915–2917 (2005).
14. U. Sunar, S. Makonnen, C. Zhou, T. Durduran, G. Yu, H. W. Wang, W. M. F. Lee, and A. G. Yodh, "Hemodynamic responses to antivascular therapy and ionizing radiation assessed by diffuse optical spectroscopies," Opt. Express **15**(23), 15507–15516 (2007).
15. M. Heckmeier, S. E. Skipetrov, G. Maret, and R. Maynard, "Imaging of dynamic heterogeneities in multiple-scattering media," J. Opt. Soc. Am. A **14**(1), 185–191 (1997).
16. T. Binzoni, T. S. Leung, D. Rüfenacht, and D. T. Delpy, "Absorption and scattering coefficient dependence of laser-Doppler flowmetry models for large tissue volumes," Phys. Med. Biol. **51**(2), 311–333 (2006).
17. G. Maret, and P. E. Wolf, "Multiple Light-Scattering from Disordered Media - the Effect of Brownian-Motion of Scatterers," Z. Phys. B Condens. Matter **65**(4), 409–413 (1987).
18. G. Yu, T. Durduran, C. Zhou, T. C. Zhu, J. C. Finlay, T. M. Busch, S. B. Malkowicz, S. M. Hahn, and A. G. Yodh, "Real-time in situ monitoring of human prostate photodynamic therapy with diffuse light," Photochem. Photobiol. **82**(5), 1279–1284 (2006).
19. C. Zhou, G. Yu, D. Furuya, J. Greenberg, A. Yodh, and T. Durduran, "Diffuse optical correlation tomography of cerebral blood flow during cortical spreading depression in rat brain," Opt. Express **14**(3), 1125–1144 (2006).
20. P. J. Berne, and R. Pecora, Dynamic Light Scattering (Wiley, New York, 1976).
21. D. A. Boas, L. E. Campbell, and A. G. Yodh, "Scattering and Imaging with Diffusing Temporal Field Correlations," Phys. Rev. Lett. **75**(9), 1855–1858 (1995).
22. D. A. Boas, and A. G. Yodh, "Spatially varying dynamical properties of turbid media probed with diffusing temporal light correlation," J. Opt. Soc. Am. A **14**(1), 192–215 (1997).
23. P. Zakharov, A. Völker, A. Buck, B. Weber, and F. Scheffold, "Quantitative modeling of laser speckle imaging," Opt. Lett. **31**(23), 3465–3467 (2006).
24. P. Zakharov, A. C. Völker, M. T. Wyss, F. Haiss, N. Calcinaghi, C. Zunzunegui, A. Buck, F. Scheffold, and B. Weber, "Dynamic laser speckle imaging of cerebral blood flow," Opt. Express **17**(16), 13904–13917 (2009).
25. P. Zakharov, A. Volker, A. Buck, B. Weber, and F. Scheffold, "Non-ergodicity correction in laser speckle biomedical imaging," Proc.SPIE 6631 (2009).
26. T. J. Farrell, M. S. Patterson, and B. Wilson, "A diffusion theory model of spatially resolved, steady-state diffuse reflectance for the noninvasive determination of tissue optical properties in vivo," Med. Phys. **19**(4), 879–888 (1992).
27. A. Kienle, and M. S. Patterson, "Improved solutions of the steady-state and the time-resolved diffusion equations for reflectance from a semi-infinite turbid medium," J. Opt. Soc. Am. A **14**(1), 246–254 (1997).
28. S. L. Jacques, "Origins of tissue optical properties in the UVA, visible, and NIR regions," OSA Trends in Optics and Photonics on Advances in Optical Imaging and Photon Migration **2**, 364–371 (1996).
29. J. R. Mourant, T. Fuselier, J. Boyer, T. M. Johnson, and I. J. Bigio, "Predictions and measurements of scattering and absorption over broad wavelength ranges in tissue phantoms," Appl. Opt. **36**(4), 949–957 (1997).
30. P. R. Bargo, S. A. Prahl, T. T. Goodell, R. A. Sleven, G. Koval, G. Blair, and S. L. Jacques, "In vivo determination of optical properties of normal and tumor tissue with white light reflectance and an empirical light transport model during endoscopy," J. Biomed. Opt. **10**(3), 034018 (2005).
31. H. W. Wang, T. C. Zhu, M. E. Putt, M. Solonenko, J. Metz, A. Dimofte, J. Miles, D. L. Fraker, E. Glatstein, S. M. Hahn, and A. G. Yodh, "Broadband reflectance measurements of light penetration, blood oxygenation, hemoglobin concentration, and drug concentration in human intraperitoneal tissues before and after photodynamic therapy," J. Biomed. Opt. **10**(1), 014004 (2005).
32. P. R. Bargo, "Optical measurements for quality control in photodynamic therapy," (OGI, 2003).
33. J. Wu, M. S. Feld, and R. P. Rava, "Analytical model for extracting intrinsic fluorescence in turbid media," Appl. Opt. **32**(19), 3585–3595 (1993).
34. M. G. Müller, I. Georgakoudi, Q. Zhang, J. Wu, and M. S. Feld, "Intrinsic fluorescence spectroscopy in turbid media: disentangling effects of scattering and absorption," Appl. Opt. **40**(25), 4633–4646 (2001).
35. W. J. Cottrell, A. R. Oseroff, and T. H. Foster, "Portable instrument that integrates irradiation with fluorescence and reflectance spectroscopies during clinical photodynamic therapy of cutaneous disease," Rev. Sci. Instrum. **77**(6), 064302 (2006).
36. A. Bogaards, H. J. Sterenborg, and B. Wilson, "In vivo quantification of fluorescent molecular markers in real-time: A review to evaluate the performance of five existing methods," Photodiagn. Photodyn. Ther. **4**(3), 170–178 (2007).
37. J. C. Finlay, D. L. Conover, E. L. Hull, and T. H. Foster, "Porphyrin bleaching and PDT-induced spectral changes are irradiance dependent in ALA-sensitized normal rat skin in vivo," Photochem. Photobiol. **73**(1), 54–63 (2001).
38. B. Kruijt, S. Kascakova, H. S. de Bruijn, A. van der Ploeg-van den Heuvel, H. J. Sterenborg, D. J. Robinson, and A. Amelink, "In vivo quantification of chromophore concentration using fluorescence differential path length spectroscopy," J. Biomed. Opt. **14**(3), 034022 (2009).
39. D. C. de Veld, M. Skurichina, M. J. Witjes, R. P. Duin, H. J. Sterenborg, and J. L. Roodenburg, "Autofluorescence and diffuse reflectance spectroscopy for oral oncology," Lasers Surg. Med. **36**(5), 356–364 (2005).
40. D. A. Bellnier, W. R. Greco, G. M. Loewen, H. Nava, A. R. Oseroff, and T. J. Dougherty, "Clinical pharmacokinetics of the PDT photosensitizers porfimer sodium (Photofrin), 2-[1-hexyloxyethyl]-2-devinyl

#126926 - $15.00 USD Received 13 Apr 2010; revised 21 Jun 2010; accepted 23 Jun 2010; published 29 Jun 2010
(C) 2010 OSA

pyropheophorbide-a (Photochlor) and 5-ALA-induced protoporphyrin IX," Lasers Surg. Med. **38**(5), 439–444 (2006).
41. B. C. Wilson, M. S. Patterson, and L. Lilge, "Implicit and explicit dosimetry in photodynamic therapy:a new paradigm," Lasers Med. Sci. **12**(3), 182–199 (1997).
42. I. Georgakoudi, M. G. Nichols, and T. H. Foster, "The mechanism of Photofrin photobleaching and its consequences for photodynamic dosimetry," Photochem. Photobiol. **65**(1), 135–144 (1997).
43. C. Sheng, P. J. Hoopes, T. Hasan, and B. W. Pogue, "Photobleaching-based dosimetry predicts deposited dose in ALA-PpIX PDT of rodent esophagus," Photochem. Photobiol. **83**(3), 738–748 (2007).
44. D. A. Bellnier, B. W. Henderson, R. K. Pandey, W. R. Potter, and T. J. Dougherty, "Murine pharmacokinetics and antitumor efficacy of the photodynamic sensitizer 2-[1-hexyloxyethyl]-2-devinyl pyropheophorbide-a," J. Photochem. Photobiol. B **20**(1), 55–61 (1993).
45. P. Vaupel, F. Kallinowski, and P. Okunieff, "Blood flow, oxygen and nutrient supply, and metabolic microenvironment of human tumors: a review," Cancer Res. **49**(23), 6449–6465 (1989).
46. A. Amelink, O. P. Kaspers, H. J. Sterenborg, J. E. van der Wal, J. L. Roodenburg, and M. J. Witjes, "Non-invasive measurement of the morphology and physiology of oral mucosa by use of optical spectroscopy," Oral Oncol. **44**(1), 65–71 (2008).
47. M. P. Bard, A. Amelink, V. N. Hegt, W. J. Graveland, H. J. Sterenborg, H. C. Hoogsteden, and J. G. Aerts, "Measurement of hypoxia-related parameters in bronchial mucosa by use of optical spectroscopy," Am. J. Respir. Crit. Care Med. **171**(10), 1178–1184 (2005).
48. R. L. P. Veen, A. Amelink, M. Menke-Pluymers, C. Pol, and H. J. C. M. Sterenborg, "Optical biopsy of breast tissue using differential path-length spectroscopy," Phys. Med. Biol. **50**(11), 2573–2581 (2005).
49. R. A. Schwarz, W. Gao, D. Daye, M. D. Williams, R. Richards-Kortum, and A. M. Gillenwater, "Autofluorescence and diffuse reflectance spectroscopy of oral epithelial tissue using a depth-sensitive fiber-optic probe," Appl. Opt. **47**(6), 825–834 (2008).
50. S. Gross, A. Gilead, A. Scherz, M. Neeman, and Y. Salomon, "Monitoring photodynamic therapy of solid tumors online by BOLD-contrast MRI," Nat. Med. **9**(10), 1327–1331 (2003).
51. T. H. Pham, R. Hornung, M. W. Berns, Y. Tadir, and B. J. Tromberg, "Monitoring tumor response during photodynamic therapy using near-infrared photon-migration spectroscopy," Photochem. Photobiol. **73**(6), 669–677 (2001).
52. D. Roblyer, R. Richards-Kortum, K. Sokolov, A. K. El-Naggar, M. D. Williams, C. Kurachi, and A. M. Gillenwater, "Multispectral optical imaging device for in vivo detection of oral neoplasia," J. Biomed. Opt. **13**(2), 024019 (2008).
53. G. A. Wagnières, W. M. Star, and B. C. Wilson, "In vivo fluorescence spectroscopy and imaging for oncological applications," Photochem. Photobiol. **68**(5), 603–632 (1998).
54. E. H. Moriyama, A. Kim, A. Bogaards, L. Lilge, and B. Wilson, "A ratiometric fluorescence imaging system for surgical guidance," Adv. Opt. Technol. **2008**, 532368 (2008).

1. Introduction

Head and neck cancer arises in the regions of the oral cavity, oropharynx, larynx and salivary glands [1]. Several treatment options that afford excellent tumor control are available including surgery, chemotherapy, radiation therapy or combinations thereof [2]. In spite of improvements in treatment schemes, they have their limitations. For example, surgery may require resection of vital functional tissue such as part of the tongue. Chemo and radiation therapies may induce permanent vasculature dysfunction and necrosis, severe toxicities and irreversible injuries to non-tumor tissue such as the oral mucosa and the salivary glands, often resulting in morbidity and severe impairment of patients' quality of life. Further, normal tissue injuries may lead to changes in applied dose quantity, and/or treatment re-schedule, which may affect treatment efficacy.

Photodynamic therapy (PDT) is an emerging treatment option for head and neck cancer. PDT has been successfully utilized for early stage head and neck squamous cell carcinomas of the oral cavity and larynx, with a high degree of preservation of vital organ functions such as speech and swallowing (reviewed in ref [3]). Since PDT is a local therapy, it is expected to induce fewer adverse side effects compared to conventional systemic therapies. It can also be applied repeatedly should a single treatment fail [3]. The efficacy of PDT is largely dependent on the hemodynamics of tumor blood flow, oxygenation, and photosensitizer (PS) uptake and photobleaching [4,5]. Tissue oxygenation is a central component for PDT since in the presence of oxygen, the PS initiates chemical reactions, which results in cellular and vascular damage in targeted tissue. Tissue oxygenation is greatly affected by functional vascular parameters such as blood flow and blood oxygenation. Functional contrast of vascular parameters may change during PDT and these changes may be useful early biomarkers for therapy outcome and planning. Therefore, it is important to monitor functional vascular

#126926 - $15.00 USD Received 13 Apr 2010; revised 21 Jun 2010; accepted 23 Jun 2010; published 29 Jun 2010
(C) 2010 OSA

related biomarkers that may affect PDT efficacy. Diffuse optical methods allow assessing these markers fast, repetitively and non-invasively, and therefore have significant advantages for monitoring PDT.

In this report, we present changes in hemodynamic parameters and drug photobleaching as a response to 2-1[hexyloxyethyl]-2-devinylpyropheophorbide-a (HPPH)-mediated PDT in a patient with a squamous cell carcinoma of the oral cavity. HPPH is a second-generation PS developed at Roswell Park Cancer Institute (RPCI) with an absorption peak wavelength of 665 nm, which allows enhanced tissue penetration depth, and with less prolonged skin photosensitivity compared to Photofrin [6]. HPPH has been used at RPCI in treating dysplasia in Barrett's esophagus and in lung cancer [7]. We have initiated a Phase I clinical trial of HPPH-mediated PDT in head and neck cancer patients to determine the maximally tolerated dose. Non-invasive diffuse optical methods were incorporated for monitoring and potentially correlating changes in measured parameters with the PDT response. To our knowledge, this is the first clinical study of HPPH-mediated PDT on a head and neck cancer patient with assessment of functional multi-parameters of blood flow, oxygenation, blood volume fraction, HPPH drug concentration and fluorescence in the same clinical setting. Our non-invasive measurements are supported by cross-linking of the signal transducer and activator of transcription 3 (STAT3), a molecular marker of accumulated PDT dose [7,8]. One parameter alone may not be a strong indicator of PDT response and multi-parameters assessed by diffuse optical methods potentially may provide accurate real-time measure of PDT responses and re-evaluate treatment plan accordingly [9].

2. Methods

2.1 Measurement protocol

The patient treatment and measurement protocol was approved by the RPCI Institutional Review Board. The lesion treated was a T1 squamous cell carcinoma of the hard palate. The patient received HPPH in dextrose 5% (D5W), 4.0 mg/m^2 infusion over 1 h. Approximately 24 h later, non-invasive measurements were done in the operating room minutes before and immediately after he received treatment light (125 Joules, 150 mW/cm^2, 665 nm; 3 cm diameter treatment field). The light source for the PDT treatment was a Coherent dye laser pumped by an Argon ion laser (Spectra Physics), and the light was delivered by a single quartz lens fiber. The treatment beam was centered on the lesion with the beam diameter slightly larger than lesion diameter. Noninvasive measurements were performed just before the PDT treatment light and biopsy, and just after the treatment completed and before the second biopsy. The total measurement times were about 5 minutes before and after PDT including signal testing and adjusting, discussion with a surgeon for probe positioning and multiple measurements at different site locations.

2.2 Diffuse optical methods

A schematic of the clinical system is shown in Fig. 1a. Non-invasive measurements were done sequentially in the order of blood flow, reflectance, and fluorescence. Diffuse Correlation Spectroscopy (DCS) was utilized to monitor blood flow as described previously [5,9–17]. To date DCS has been successfully employed in the therapy monitoring field, such as PDT [5,18], chemo-radiation of head and neck [9], and chemotherapy of breast [19]. The blood flow instrument had a 785nm, long coherence length laser (CrystaLaser), four photon-counting detectors (Perkin-Elmer), and a custom built autocorrelator board (Correlator.com) (Fig. 1a). The source light was delivered to the tissue by a multi-mode source fiber. Four single-mode detector fibers were used to collect the light. Photodetector outputs were fed into a correlator board and resulting intensity autocorrelation functions and photon arrival times were recorded by a computer [5,9]. From the normalized intensity autocorrelation function, $g_2(r,\tau)$, the diffuse electric field temporal autocorrelation function ($g_1(r,\tau)$), was extracted by using Siegert relation [20], $g_2(r,\tau) = 1 + \beta|g_1(r,\tau)|^2$. Here, r is the source detector separation, τ is the autocorrelation time delay, and β is a constant related to experimental parameters such

#126926 - $15.00 USD Received 13 Apr 2010; revised 21 Jun 2010; accepted 23 Jun 2010; published 29 Jun 2010
(C) 2010 OSA

as detected number of speckles. In our analysis we obtained $\beta \sim 0.5$ by fitting but it could also be obtained experimentally from the intercept of $g_2(r,\tau)$ as the delay time τ approaches zero. It was shown that the electric field autocorrelation function satisfies the correlation diffusion equation and one can extract analytical solutions in reflectance geometry similar to solutions obtained by solving diffusion equation [21,22]. It can be shown that the temporal decay rate of the electric field autocorrelation function is a function of optical parameters and αD_B, if one assumes the effective blood flow speed is characterized by effective diffusion coefficient (D_B) for the blood cells [11,14,19]. Here, α is the probability that a scattering event in tissue is from a moving scatterer, and is roughly proportional to tissue blood volume fraction (*BVF*). Therefore, αD_B characterizes blood flow and higher decay rate correlates with higher blood flow (Fig. 2a) [11,12,22]. It should be noted that optical parameters were obtained by diffuse reflectance measurements and supplied as prior information in quantification of blood flow related parameter. In this report, we introduce *rBF* for blood flow changes due to PDT: *rBF* is a blood flow parameter measured relative to its pre-treatment value, i.e. $rBF = BF_{post}/BF_{pre}$. We assumed our system was ergodic, which may not be true in reality; more generalized schemes of non-ergodic systems have been investigated recently [23–25].

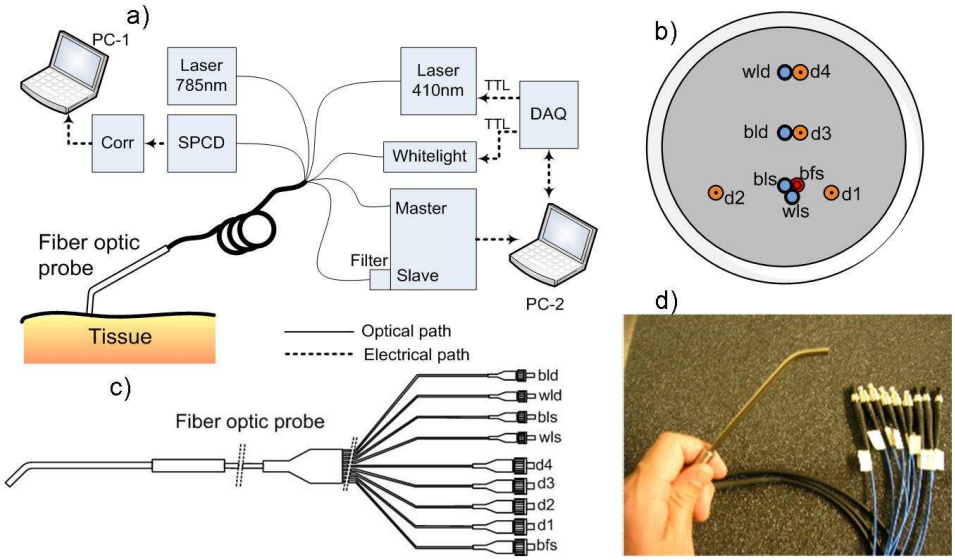

Fig. 1. Schematic diagram of the instrument and fiber optic probe. a) The combined DCS, DFS and DRS setup with fiber optic probe. DCS consists of 785 nm laser, single photon counting detector (SPCD), a custom correlator (Corr), and a laptop (PC-1). DFS and DRS mainly consist of a dual channel spectrometer, 410 nm blue laser and a whitelight source. Data acquisition card (DAQ) switches the blue and whitelight sources via a laptop (PC-2). b) Diagram of source-detector fiber configuration. bfs: the blood flow laser, d1,..d4 are DCS detector fibers, wls: white light source fiber, bls: blue light source fiber, bld: blue light detector fiber, wld: white light detector fiber. The distances between bfs-d1, bfs-d2, bfs-d3, and bfs-d4 are 0.6, 1.2, 0.8 and 1.6mm, respectively. The distance between wls-wld is 1.6mm and that between bls-bld is 0.8mm. c) Diagram of the fiber optic probe. d) Picture of the probe.

After blood flow measurements, the second laptop initiated consecutive fluorescence and reflectance data acquisition by utilizing TTL switching via a data acquisition card (DAQ, National Instruments). In absorption mode, broadband diffuse reflectance measurements were taken by exciting the tissue with tungsten halogen lamp (Ocean Optics) and collecting the light with the Master channel of a two channel spectrometer (Ocean Optics). In fluorescence mode, a 410 nm laser diode with 4mW laser power (Power Technology) excited the HPPH in Soret band and the Slave channel of the spectrometer collected the HPPH fluorescence above 500 nm. A hand-held probe secured the source and detector fibers of the instruments. The probe had a single large ferrule holding all the fibers (FiberOptic Systems, Inc.). For source

#126926 - $15.00 USD Received 13 Apr 2010; revised 21 Jun 2010; accepted 23 Jun 2010; published 29 Jun 2010
(C) 2010 OSA

and detector fibers, 400 μm, multimode fibers were used except for the detector fibers of the blood flow instrument, wherein 5 μm single mode detection fibers were used to collect only a few speckles in the investigated tissue. Source detector separations were 1.6 mm for reflectance, 0.8 mm for fluorescence and 0.6, 0.8, 1.2 and 1.6 mm for DCS (Fig. 1b). The total probe diameter was 5mm and the wall thickness of the probe was 0.5mm. The probe tip was angled by 45° (Fig. 1c, d) and the probe face was polished at an angle of 8° for better contact and to minimize specular reflection in the oral cavity. The probe tip was sterilized with alcohol before and after each measurement. The probe slightly touched the tissue surface to make good physical contact. Due to time constraint in the operating room (OR), three repeated measurements were carried out from normal tissue (outside of the treated tumor area) and three (pre-PDT) and five (post-PDT) independent measurements were taken from tumor tissue to investigate the statistical power and repeatability of our non-invasive measurements. Independent measurements were obtained by putting the hand-held probe each time at slightly different spatial positions.

For the analysis of reflectance data, background subtracted tissue reflectance was normalized by a diffuse reflectance standard (Ocean Optics) to obtain measured normalized reflectance (Fig. 2b). An analytic diffuse reflectance modeling [26,27] and Levenberg-Marquardt (lsqnonlin, Matlab) algorithm was utilized to fit the model to experimental data. We assumed absorption coefficient, $\mu_a(\lambda)$, composed of linear contribution from blood, water, and HPPH absorption:

$$\mu_a(\lambda) = BVF \times (StO_2 \times \mu_a^{oxy}(\lambda) + (1 - StO_2) \times \mu_a^{deoxy}(\lambda)) + wf \times \mu_a^{water}(\lambda) + C_{HPPH} \times \mu_a^{HPPH}(\lambda), \quad (1)$$

where μ_a^{oxy}, μ_a^{deoxy}, μ_a^{water}, μ_a^{HPPH} are the absorption coefficients of oxy-hemoglobin, deoxy-hemoglobin, water and HPPH, respectively. *BVF* is the blood volume fraction, StO_2 is the blood oxygen saturation, *wf* is the water fraction, and C_{HPPH} is the HPPH concentration. Tissue scattering was also assumed to have Mie type behavior, $\mu'_s(\lambda) = A\,\lambda^{-b}$, where *A* and *b* are related to scatterer size and concentration [28,29]. A multi-wavelength fitting algorithm that fits all 798 wavelengths in the range of 520 nm to 820 nm simultaneously was applied to directly extract *bvf*, StO_2, C_{HPPH}, *A*, *b* [30–32]. Water contribution was assumed small in this wavelength range and *wf* was fixed to 0.70.

For the analysis of diffuse fluorescence spectroscopy (DFS), the fluorescence signal intensity was normalized by the acquisition time of CCD and background subtracted tissue fluorescence was normalized by diffuse reflectance spectra [33–36]. Normalized tissue fluorescence ($Fn(\lambda)$) was modeled as linear contributions of HPPH fluorescence ($F_{HPPH}(\lambda)$) and autofluorescence ($F_{af}(\lambda)$) [35,37,38]:

$$Fn(\lambda) = C_{HPPH} \times F_{HPPH}(\lambda) + C_{af} \times F_{af}(\lambda). \quad (2)$$

Here C_{HPPH} and C_{af} are spectral amplitudes of HPPH and background autofluorescence, respectively. HPPH fluorescence spectra basis was obtained by measuring HPPH in a cuvette and autofluorescence basis was obtained by averaging five independent measurements from a patient prior to HPPH administration (Fig. 2d). Figure 2c shows the representative measured tumor fluorescence having HPPH fluorescence spectra component between 600nm and 800nm wavelength range with a peak at 668nm and background autofluorescence component, which possibly originated from several endogenous fluorophores such as collagen, elastin, keratin, and reduced nicotinamide adenine dinucleotide (NADH) [39]. In our analysis, measured tissue fluorescence data from 600nm to 800nm were fitted (lsqnonlin, Matlab) to extract C_{HPPH} and C_{af} and changes in C_{HPPH} due to photobleaching is reported in the Results section (Fig. 3e).

#126926 - $15.00 USD Received 13 Apr 2010; revised 21 Jun 2010; accepted 23 Jun 2010; published 29 Jun 2010
(C) 2010 OSA

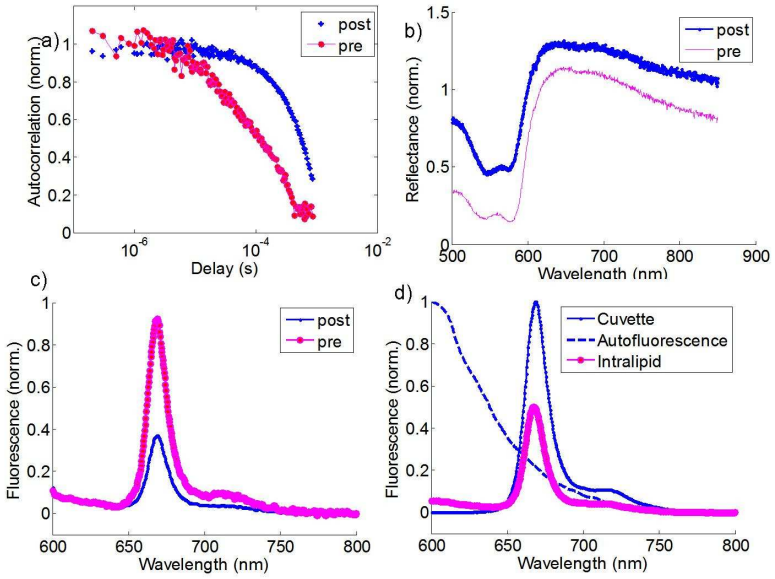

Fig. 2. a) Representative curves (tumor site) of normalized autocorrelation functions, $g_1(r,\tau)$ (decay rate is related to blood flow) b) normalized DRS data and c) normalized fluorescence pre- and post-PDT. d) HPPH spectra obtained in cuvette, autofluorescence spectra obtained from a patient, and HPPH spectra from an oral tissue simulating phantom. Cuvette and autofluorescence data is normalized to 1. Intralipid data is normalized to 0.5 for better view compared to cuvette data.

2.3. STAT3 crosslinking analysis

A tumor biopsy was taken from the PDT-treated region for Western blotting (Fig. 3f) within minutes after non-invasive optical measurements were completed. The oxidative cross-linking of STAT3 as a function of photoreaction in the treatment field was determined as described elsewhere [7,8]. Briefly, the tissue sample was homogenized and extracted proteins were separated on 6% SDS-polyacrylamide gels. The proteins were transferred to nitrocellulose membranes and reacted overnight with antibodies to STAT3 (Santa Cruz Biotechnology). Detection of immune complexes was performed by using enhanced chemiluminescence (ECL) (Pierce Chemical). ECL images were recorded on X-ray films and pixel values at each band were integrated using the ImageQuant TL program (Amersham Biosciences). PDT-induced cross-linking was expressed as the percentage conversion of monomeric STAT3 into the dimeric complex I. FaDu (human hypopharyngeal carcinoma) cells, treated in vitro with 200 nanomol/ml HPPH and 3 J/cm^2 of 665 nm light, were used as positive control.

3. Results and discussion

Figure 3a shows that mean tumor blood flow (*rBF(%)*) decreased by ~85% whereas normal tissue did not show such a trend. Reduction in blood flow was accompanied by corresponding changes in blood volume fraction (*BVF* (%)) and blood oxygen saturation (StO_2 (%)). We note from Fig. 3b that the mean baseline value of *BVF* (~2.9%) is close to previously published data for the head and neck tumors in oral region [32]. After PDT, *BVF* decreased to the level of ~1.7%. We also observed a decrease in normal tissue but to a smaller extent. Changes in normal tissue may be due to physiological fluctuations in the OR during PDT and/or due to tissue sampling difference during our point measurements before and after PDT. Our data showed significant decrease in mean tumor blood oxygen saturation (StO_2 (%)) after PDT (Fig. 3c) from ~76% to ~36%, but StO_2 in normal tissue was fairly constant. These results

#126926 - $15.00 USD Received 13 Apr 2010; revised 21 Jun 2010; accepted 23 Jun 2010; published 29 Jun 2010
(C) 2010 OSA

suggest that HPPH-PDT induced significant vascular changes in tumor tissue, confirming previous observations of vascular disrupting effects by HPPH [40].

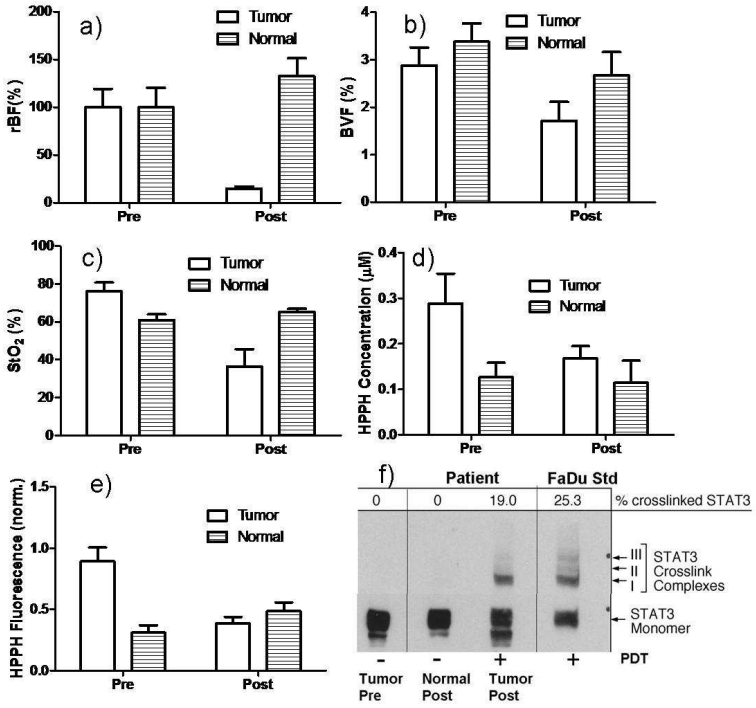

Fig. 3. Extracted functional parameters from a head and neck patient before and after PDT. a) Relative blood flow (*rBF*(%)). b) Blood volume fraction (*BVF* (%)). c) Blood oxygen saturation (*StO2* (%)). d) HPPH concentration (μM). e) HPPH fluorescence (normalized). f) STAT3 cross-linking.

Another useful parameter for monitoring PDT is to monitor changes in the PS. PS preferentially accumulates in tumor tissue compared to normal tissue [41]. During PDT, PS may photobleach due to several possible mechanisms (e.g. generation of singlet oxygen) [41,42] and PS photobleaching may play an important role in determining deposited PDT dose [41–43]. HPPH drug uptake could be quantified by analyzing reflectance spectra. As Fig. 1d shows, reflectance spectra exhibited a small dip at ~665 nm, at HPPH absorption peak above 500 nm wavelength (above Soret band) region. Multi-wavelength fitting algorithm allowed simultaneous quantification of absolute HPPH drug concentration and vascular parameters. Our results (Fig. 3d) showed higher HPPH uptake in tumor compared to normal tissue. The tumor to normal tissue ratio of the drug uptake was ~2.3, a value that is within the previously published range [44]. After PDT, HPPH drug concentration at the tumor site decreased due to photobleaching by ~41%, whereas normal tissue drug concentration was similar to the pre-PDT value.

We also utilized the sensitive technique of fluorescence spectroscopy to assess PS photobleaching *in vivo* [37,41]. Figure 3e indicates normalized HPPH fluorescence amplitude (C_{HPPH}) was about ~2.8 times higher in tumor compared to normal tissue before PDT, and exhibited a decrease (~56%) due to photobleaching, supporting the HPPH concentration data obtained from diffuse reflectance measurements. The slight differences between diffuse fluorescence and reflectance trends may be due to differences in drug accumulation in different layers of oral tissue, light penetration, source detector separations, and optical properties.

#126926 - $15.00 USD Received 13 Apr 2010; revised 21 Jun 2010; accepted 23 Jun 2010; published 29 Jun 2010
(C) 2010 OSA

We have shown previously in preclinical models and biopsy material obtained from non-small cell lung cancer patients that conversion of STAT3 monomer to STAT3 crosslinked complexes is related to accumulated PDT dosage and can be a quantitative biomarker of cellular killing [7,8]. Tumor analysis showed maximal STAT3 conversion to cross-links of ~25% with a median of ~12% [7]. Biopsy tissue analyzed from this patient showed 19.0% STAT3 conversion (Fig. 3f), suggesting an effective accumulated PDT dose.

This study particularly focused on the *changes* in functional parameters due to PDT, but it may also be valuable to look into a possible correlation of pretreatment levels and PDT efficacy in the future. If we compare between tumor and normal tissue, we see that tumor hemodynamic parameters were similar to normal values at pretreatment. It is believed that malignant tumors normally show higher blood flow and blood volume and lower oxygen saturation [45]. Certainly it is not easy to make conclusive remarks from one patient data but there may be several possible explanations. It is possible that normal tissue measured away from the tumor and treatment area was not representative of normal tissue adjacent to the tumor. In our ongoing studies we will measure a region close enough to tumor tissue so that it will get PDT treatment light but also far enough so that it can safely be regarded as normal tissue. It is also possible that the depth and the thickness of the tumor were small so that DRS and DCS probed more stroma tissue below the tumor compared to DFS, which probed superficial tumor in a greater extent due to its shorter source-detector separation and wavelength. Differential path-length spectroscopy, a technique for preferential detection of superficial photons at shallow depths, has shown significant differences in StO_2 and *bvf* in oral mucosa [46], bronchial mucosa [47], and breast tissue [48]. In general, it would be beneficial to have a depth sensitive probe with variable source detector separations as demonstrated recently [49]. Depending on its stage, it might happen that this tumor did not have contrast in vascularization but had higher StO_2. A high level of StO_2 may have therapeutic benefits since oxygen is required for PDT.

In this study diffuse optical measurements were done at two time points: just before and just after PDT treatment. It is desirable to do concurrent, real-time measurements during PDT and a while after PDT. Previous studies showed that real-time measurements during PDT can provide predictive information [5,18,35,38,41,43,50,51]. It is possible to "filter-out" the treatment light during non-invasive measurements to extract noninvasive parameters during PDT. However, concurrent measurements are a real challenge, because optical probes might introduce a risk of interrupting treatment light and time constraints for fine adjustments for both treatment and measurement inside the OR. Compared to flat surface applications such as subcutaneous tumor models and skin, head and neck region has more space constraints for probe positioning. Further, tumor locations may differ significantly for each patient, which may require different types of treatment fibers for each case; thus requiring adaptation of fiber-optic probe accordingly. Non-contact camera [52] and endoscope [53,54] based probes may allow concurrent measurements for easily accessible tumors in the head and neck region. Measurements taken a while after PDT were avoided due to time constraints in the OR. Outside of the OR measurements were also avoided, because baseline blood flow values might be affected due to anesthesia and temperature effects. Further, unavailability of the surgeon outside of the OR could jeopardize the ability to coregister the measurement locations.

4. Conclusion

We presented preliminary results of photobleaching and changes in vascular parameters due to HPPH-mediated PDT in a recently initiated clinical study for head and neck cancer patients by utilizing non-invasive, fast diffuse optical techniques. HPPH-mediated PDT induced significant photobleaching and vascular destruction, causing substantial reduction of drug concentration, blood flow, oxygenation and blood volume fraction. The data indicate a qualitative agreement between non-invasive diffuse optical methods and a biopsy-based molecular marker, both reporting on photodynamic efficiency. Each parameter showed variable sensitivity to the therapy for this particular patient, thus emphasizing the need for

#126926 - $15.00 USD Received 13 Apr 2010; revised 21 Jun 2010; accepted 23 Jun 2010; published 29 Jun 2010
(C) 2010 OSA

simultaneous monitoring of multiple tissue parameters and the potential for individualized treatment planning. Therefore, extracted multi-parameters should be valuable for understanding and assessing the PDT dose adjustment and clinical response. Molecular analysis of the PDT reaction and non-invasively obtained functional parameters presented here have potentials to complement and support each other in evaluating PDT efficacy. The ongoing clinical trial and collection of data generating statistically significant data sets will assist in this endeavor.

Acknowledgements

This paper is dedicated to the memory of Dr. Allan Oseroff. This research is supported by RPCI Startup Grant (U. Sunar) and NCI CA55791 (B. W. Henderson). We are grateful to Dr. R. K. Pandey for providing the HPPH drug.

#126926 - $15.00 USD Received 13 Apr 2010; revised 21 Jun 2010; accepted 23 Jun 2010; published 29 Jun 2010
(C) 2010 OSA